RSC Advances

ROYAL SOCIETY OF CHEMISTRY

www.rsc.org/advances

Graphical Abstract

Multi walled carbon nanotube buckypapers and their hybrids with Ag nanoparticles have been fabricated with the assistance of polybenzimidazole.

Polybenzimidazole assisted fabrication of multiwalled carbon nanotube buckypapers and their silver nanoparticle hybrids

Yanli Zhang[a], Yan Wang*[b], Junrong Yu[a], Lei Chen[b], Jing Zhu[b]

and Zuming Hu*[a]

a State Key Laboratory for Modification of Chemical Fibers and Polymer Materials,

Donghua University, 201620, Shanghai (P. R. China)

b College of Material Science and Engineering, Donghua University, 201620, Shanghai (P.

R. China)

*Corresponding authors. Tel.: +86-21-67792944. Fax: +86-21-67792945.

E-mail: wy@dhu.edu.cn (Y. Wang);   hzm@dhu.edu.cn (Z. Hu)

Abstract

Buckypapers represent an attractive form of macroscopic material of carbon nantubes with promising applications in electronics, microfilters, and composites, etc. The deposition of metal nanoparticles on buckypaper can further endow buckypapers with multifunctionalities such as unique optical, magnetic and catalytic properties. The homogenous dispersion and proper surface functionalization of carbon nanotubes are key factors for realization of high-performance buckypapers and their multifunctional metal hybrids. To this goal, this work reports the fabrication of multi walled carbon nanotube (MWNT) buckypapers and their silver nanoparticle (AgNP) hybrids with the assist of a high-performance polymer, polybenzimidazole (PBI) for the first time. By optimizing the dispersion conditions of MWNTs in organic solvent with PBI as a non-covalent modifier, highly concentrated dispersions of homogenously dispersed MWNTs can be obtained, thus facilitate the subsequent fabrication of buckypapers by filtration method. The resultant MWNT/PBI papers show good mechanical and thermal properties due to the excellent intrinsic properties of PBI and the strong interactions between MWNTs and PBI. The effect of processing parameters of MWNT dispersions on the final performance of buckypapers was also evaluated. Making use of the coordination effect of imidazole groups to metal ions, AgNPs with relatively uniform sizes were then deposited on surfaces of MWNTs/PBI buckypaper. The Ag/buckypaper hybrid was found to be highly active and reusable catalyst for reduction of 4-nitrophenol.

1.Introduction

Carbon nanotube (CNT) has gained extensive attention since its discovery in1990s for its excellent mechanical properties, conductivities, thermal and chemical stabilities, etc. Since then, great efforts have been devoted to making use of these advantages of CNTs in real applications. With this respect, a prerequisite is to construct macroscopic materials based on CNTs. Incorporation of CNTs into polymer matrix to fabricate CNT/polymer composites is a frequently adopted strategy to achieve this goal[1-3]. However, since the homogeneous dispersion of CNTs in polymer composites is difficult to achieve, the addition amount of CNTs in polymer matrix is usually very small, which poses a great challenge to exploitation of the full potential of CNTs[4-6]. Assembly of CNTs, such as two-dimensional CNT buckypaper, is another class of macroscopic CNT-based material that has great potential in applications of electronics, filtration, and composites[7-10]. As the major components in these materials are CNTs, they exhibit superior electrical or thermal properties as compared to CNT/polymer composites[11-15].

Solution-based filtration is a simple and economic way to make free standing CNT buckypapers with commercially available CNTs as starting materials. However, due to the inert surfaces of CNTs, it is hard to prepare homogeneous dispersion of CNTs in common solvents, as well as CNT papers with both good mechanical stability and electrical conductivity. Therefore, surface modification of CNTs prior to solution-processed assembly is necessary to prepare robust buckypapers[16-20]. The surface modification could not only

separate individual tubes from agglomerates that facilitate the fabrication of homogeneous

CNT buckypapers, but also strengthen the intertube interactions. In this regard,

non-covalent modification of CNTs with polymers is advantageous because: 1) in

comparison to covalent modification, non-covalent method could preserve the conjugated

structure of CNTs; 2) as compared to some modification agents of small molecules,

polymers provide better stabilities to the modified buckypaper. As a result, many common

surfactants[21] or polymers have been used to reinforce CNT buckypaper, such as

polyvinylpyrrolidone[22], poly(allylamine)[23], and some biopolymers[24, 25]. However, from

previous works, it can be seen that most of polymers used are water-soluble. Although

water-soluble polymers could permit the fabrication of CNT buckypaper in

environmentally-friendly aqueous solution, the susceptibility of these polymers to moisture

would restrict the use of CNT buckypaper in wet conditions. Moreover, CNT buckypaper

reinforced with water-soluble polymers could hardly be used in high-temperature or some

harsh conditions because of the poor thermal and chemical stabilities of these water-soluble

polymers. It is also noted that there were some reports dealing with non-water soluble

polymers reinforced buckypaper, such as epoxy resin[7, 26, 27], polycarbonate[28, 29],

poly(phenylene sulphide) and poly(ether ether ketone)[30, 31]. However, for these composites,

buckypapers should be pre-synthesized by surfactant-aided dispersion and filtration, then

the surfactant was removed by repeated washing and the polymers were infiltrated into the

resultant buckypapers, which makes the fabrication process complex.

Decoration of CNT buckypapers with metal nanoparticles (MNPs) could further improve their electrical conductivity, and broaden the use of buckypapers in novel applications such as catalysis, energy, and sensors because of the unique optical, electronic, magnetic and catalytic properties of MNPs as compared to their bulk counterparts[32-35]. With regard to MNPs, the physical and chemical properties directly related to their sizes and dispersion. However, MNPs tend to aggregate due to their high surface energy, which would compromise their excellent properties. Therefore, designing MNPs with long-term dispersion stability is highly important for their use in practical applications. Fixation of MNPs on solid supports, such as carbon spheres[36], electrospun nanofibers[37], or graphene papers[38], is a strategy that has been widely adopted to protect MNPs against aggregations and maintain their activity. In this respect, immobilizing MNPs onto CNT buckypapers could not only make these papers more conductive and multifunctional, but also make MNPs highly disperse and easy recovery in applications such as heterogeneous catalysis. Surface modification of CNT is again a crucial step to improve the interactions between CNTs and MNPs, and obtain highly integrated and stable MNP/CNT hybrid paper. In addition, mechanical, chemical and thermal stabilities of the paper substrate are equally highly important for reliable use of MNP/CNT hybrid paper.

Based on the above-mentioned consideration, herein, we report the fabrication of mechanically robust, chemically and thermally stable multiwalled carbon nanotube (MWNT) buckypaper, and their hybrids with silver nanoparticles (AgNPs). The key of this

work is the selection of polybenzimidazole (PBI) as dispersant for non-covalent

modification of MWNTs, and glues for buckypaper. PBI is a kind of high-performance

heteroaromatic polymer with good mechanical properties as well as excellent thermal and

chemical stabilities in comparison to traditional plastics. Some of us have previously

demonstrated the advantages of the combination of PBI and carbon nanomaterials[39, 40].

Works conducted by Nakashima et al. also demonstrated that PBI could adhere to surfaces

of MWNTs via π-π interactions[41-43], therefore, it is expected that the exploitation of the

merits of PBI in buckypapers could enable us to prepare stronger and more stable

buckypapers. In fact, we note that high-performance aromatic polymers were scarcely

reported for this purpose. Another important reason for the choice of PBI is that in contrast

to the non-polar characteristics of many other high-performance polymers, the active

imidazole groups in PBI chains could coordinate with metal ions[44-46], thus facilitate the

immobilization of MNPs on MWNT papers. AgNPs were chosen as model MNPs because

they were cost-effective with good catalytic and antibacterial properties[47-49]. In this paper,

we first optimized the preparation condition for buckypapers and investigated their

mechanical, electrical and thermal properties, then we have in-situ deposited AgNPs on

buckypapers and evaluated the use of Ag/buckypaper hybrid as reusable catalyst for

reduction of 4-nitrophenol.

2. Experimental Section

2.1. Materials.

MWNTs with diameters of 10-15 nm and lengths of 10-20 μm were supplied by Chengdu Organic Chemicals Co. Ltd. 3,3'-Diaminobenzidine (DABz) and isophthalic acid (IPA) were purchased from J&K Chemical in Shanghai. Polyphosphoric acid (PPA)、phosphorus pent-oxide (P_2O_5), N,N-Dimethylacetamide (DMAc), silver nitrate ($AgNO_3$), 4-nitrophenol (4-NP), sodium borohydride ($NaBH_4$), and hydrazine hydrate were purchased from Alfa Aesar and used as received. PBI was synthesized by direct polycondensation of DABz and IPA in P_2O_5/PPA solution as previous reported[50], the chemical structure of PBI is shown in Figure 1. The intrinsic viscosity of PBI was measured to be 1.0255 dL g^{-1} in 98 wt% sulfuric acid solution using an Ubbelohde viscometer at 30 °C. The molecular weight of PBI was thus calculated to be 50900 based on Mark–Houwink–Sakurada equation[50].
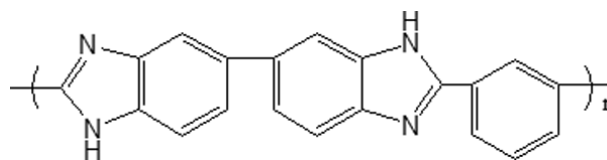
Figure 1. Chemical structure of PBI.

2.2 Fabrication of MWNT-based buckypapers

Prior to the fabrication of buckypapers, MWNTs should be homogenously dispersed in solvents. Therefore, we first optimized the dispersion of MWNTs in DMAc with the aid of PBI. In typical experiments, PBI was dissolved in 10 mL DMAc completely, then required amount of MWNTs were added in the solution. The mixture was subjected to high-power

tip sonication for 5 min and low-power bath sonication for 2 h. After centrifugation at 954 g

for 10 min, homogenous dispersions of MWNTs were obtained. Buckypapers were

prepared by traditional filtration method. The dispersion of MWNTs were filtrated through

a polytetrafluoroethylene (PTFE) membrane with pore size of 0.22μm and diameter of 47

mm. Then large amount of pure DMAc was filtrated through the formed buckypapers to get

rid of loosely bounded PBI. After washing, the buckypapers were dried at 80 °C in vacuum

overnight. The dried buckypapers were then carefully peeled off from the underlying PTFE

membrane.

2.4 Fabrication of Ag/buckypaper hybrids

In a typical synthesis, the buckypaper was immersed into aqueous solution of $AgNO_3$

(2.5mg/mL) with slight shaking for a particular time at room temperature. After that,

buckypaper was washed with water for several times and dipped into dilute hydrazine

hydrate solution to reduce the adsorbed Ag ions into AgNPs.

2.5 Characterization

UV-vis spectra were measured on a Perkin-Elmer Lambda 35 UV/vis spectrometer.

Transmission electron microscopy (TEM) images were obtained using JEM-2100. SEM

images were obtained using scanning electron microscope (FE-SEM) (S-4800, HITACHI

Ltd, Japan). Element Analysis were taken with an Vario EL III CHNS analyzer (Elementar,

Germany), samples were combusted at high temperature in oxygen-rich environment, the

combustion gas were analyzed to measure the elements of C, H and N, element O was then

calculated by difference. Raman spectra was taken with Renishaw Micro-Raman Spectroscopy (inVia-Reflex), equipped with a holographic grating of 1800 lines mm^{-1} and a He-Ne laser (633 nm) as excitation source. Thermogravimetric analysis (TGA) was performed in area with a Netzsch TGA 209 F1 instrument at a heating rate of 20 °C min^{-1}. The tensile properties of buckypapers and Ag/buckypaper hybrids were measured with a WDW3020 instrument at room temperature with humidity about 50% at a crosshead speed of 1 mm min^{-1}, the initial gauge length is 30 mm. The conductivities of papers were measured by a standard four-probe method. X-ray diffraction (XRD) patterns were collected in a D/max-2550 PC instrument.

The catalytic activity of the Ag/buckypaper hybrid was tested by a model reaction, which is the reduction of 4-NP with $NaBH_4$ as the redactant. After mixing the homogeneous solution of 4-NP (0.2 mL, 0.1 mM) and $NaBH_4$ (0.8 mL, 1 mM) with de-ionized water (3 mL) in quartz cuvette, Ag/buckypaper hybrid (1 mg) was added. Meanwhile UV-Vis spectra were recorded in the sequence of time to monitor the reduction of 4-NP.

3. Results and Discussion

3.1. Optimizing the dispersion of MWNTs/PBI in DMAc.

Homogeneous dispersion of MWNTs in solvent is necessary to prepare buckypaper with good properties, because the aggregations of MWNTs could act as stress concentration points that weaken the buckypaper. PBI has previously been used for non-covalent modification of MWNTs, the conjugated backbone of PBI was demonstrated to interact

with MWNTs via π-π interactions[41-43]. However, the solution behavior of MWNTs in PBI

solution was not reported and the optimal condition for dispersion of MWNTs was

unknown. Therefore, we first investigated the dispersion of MWNTs/PBI in DMAc, which

was a good solvent for PBI.

Figure 2a visually demonstrated the dispersion ability of PBI to MWNTs. When

unmodified MWNTs were dispersed in DMAc and allowed to stand for one week, most of

the MWNTs aggregated and precipitated at the bottom of the vial even with concentration

as low as 0.01 mg/mL. The addition of PBI resulted in more homogeneous dispersions of

MWNTs, as shown in Figure 2a. At low MWNT concentration (0.01 mg/mL), MWNTs/PBI

dispersed homogenously in solution. As the concentration of MWNTs increased to 1

mg/mL, thicker dispersion was obtained. However, we also noted that a portion of MWNTs

were settled at the bottom, suggesting the necessity to optimize the dispersion condition of

MWNTs to prepare concentrated dispersion of MWNTs, which would facilitate the

subsequent fabrication of MWNT-based macroscopic materials.

To this end, we quantitatively evaluated the effect of PBI concentration and initial

MWNT concentration on the final concentration of dispersed MWNTs in solution, while

kept the sonication time and centrifugation force (954 g) constant. UV-vis absorbance

measurements was used to measure the efficacy of PBI at dispersing MWNTs. MWNT

concentrations could be determined by the Beer-Lambert law, $A = \varepsilon l c$, where A was the

absorbance at a given wavelength, ε was the extinction coefficient, l was the light path

length, and *c* was the MWNT concentration. The ε was determined by plotting the absorbance at wavelength of 500 nm of very dilute and well-dispersed MWNTs/PBI (mass ratio 1:1) dispersions against their concentrations. The inset of Figure 2c shows that there is a good linear relationship (with *R*= 0.9998) between the absorbance and concentration of MWNTs, the extinction coefficient thus obtained was 0.05447 L mg^{-1} cm^{-1}, which was slightly higher than previously reported value for MWNTs in DMAc[51].

Using ε for MWNTs/PBI dispersion, the concentrations of MWNTs can be determined, as shown in Figure 2d to 2f. When fixed the concentration of MWNTs as 1 mg/mL, while varied the dosage of PBI, we found the optimal concentration of PBI was 1 mg/mL. With this concentration of PBI, the concentration of MWNTs in resultant dispersion was 0.247 mg/mL. Further increasing of PBI resulted in lower concentration of dispersed MWNTs, which might be due to the higher viscosity. When fixed the PBI concentration as 1 mg/mL, the highest concentration of dispersed MWNTs achieved was 1.610 mg/mL with the initial MWNT concentration of 9 mg/mL. Further increasing of initial concentration of MWNTs resulted in decrease in concentrations of dispersed MWNTs. Notably, when the initial concentration of MWNT reached 15 mg/mL, almost no MWNTs remained in dispersion. This might be due to the fact that too high concentration of MWNTs in solution would result in no free space to separate individual tubes from agglomerates. In addition, the effect of centrifugation force was also evaluated, the maximum concentration of MWNTs decreased from 1.610 to 1.309 mg/mL as the centrifugation force increased to 3819 g, and

further decreased to 0.897 mg/mL as the centrifugation force increased to 8594 g. However, despite the different concentrations achieved by different centrifugation force, all dispersions were stable even for weeks, demonstrating well-dispersed MWNTs could be obtained at all the tested centrifugation force.
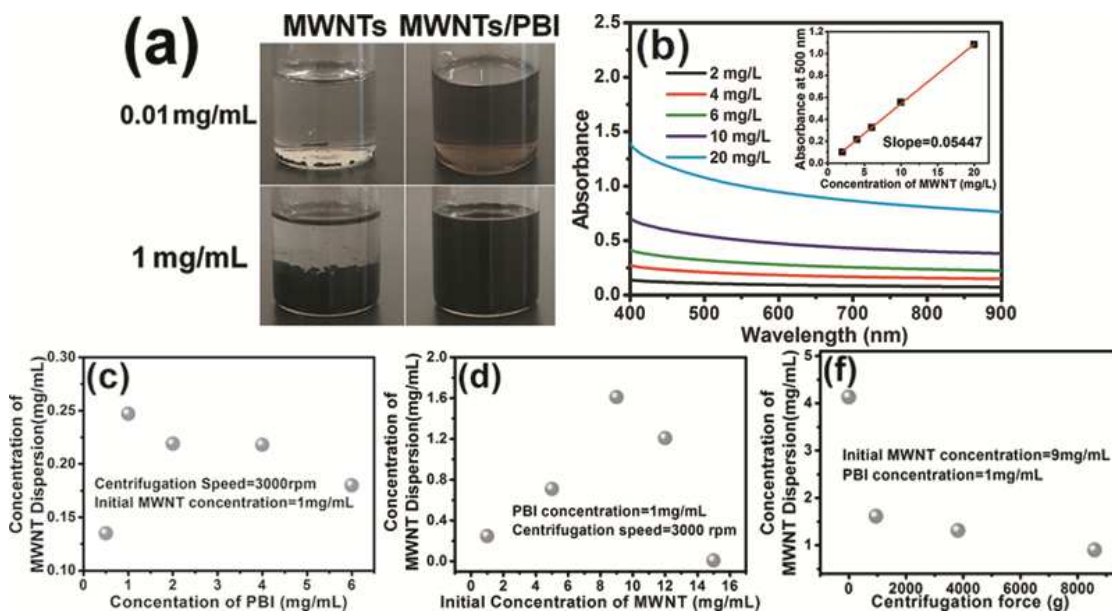
Figure 2. (a) Photographs of MWNTs and MWNTs/PBI (mass ratio = 1:1) dispersions. (b) Absorption spectra of MWNTs/PBI (mass ratio = 1:1) in DMAc at different MWNT concentrations. Inset shows the absorbance of these dispersion at 500 nm. (c) Effect of PBI concentrations on the concentration of dispersed MWNTs in solution. (d) Effect of initial concentrations of MWNTs on the concentration of dispersed MWNTs in solution. (e) Effect of centrifugation force on the concentration of dispersed MWNTs in solution.

12

To better get the dispersion state of MWNTs and PBI-dispersed MWNTs in DMAc , we characterized the dispersions obtained at different centrifugation force by TEM, as shown in Figure 3. It was found that MWNTs formed large aggregates (Figure 3a), which was not disentangled simply by sonication in solvent. Some impurities, which appeared as black dots, could also be found in Figure 3a. While most PBI dispersed MWNTs appeared as individual tubes due to the non-covalent binding of PBI on the sidewalls and the removal of non-disentangled MWNT aggregations (Figure 3c, 3e, and 3g) by centrifugation. At higher magnification, the MWNT surface was smooth (Figure 3b), while there were some amorphous lumps, which we attributed to the attached polymers that contributed to the stability of MWNTs in dispersions on surfaces of PBI dispersed MWNTs. Moreover, it was found that the attached polymers increased with increasing of centrifugation force (Figure 3d, 3f, and 3h), suggesting MWNTs with less attached PBI were removed at higher centrifugation force. Some short tubes could also be found in Figure 3e and 3g, demonstrating shorter tubes were more stable against centrifugation, which could be expected as heavier objects always settled faster than lighter ones. Based on the TEM characterization, we assumed that the centrifugation force should affect the final performance of buckypaper because of the different amount of adsorbed polymers and different morphologies of MWNTs in dispersions. Therefore, in the next step, we have prepared three buckypapers from dispersions obtained at centrifugation force of 954, 3819, and 8594 g, which were named MBP-1, MBP-2, and MBP-3, respectively. Buckypaper

made from unmodified MWNT (MBP) was also tested for comparison. It should be noted

that the mass of MWNTs in each papers was set to be 30mg, and the thicknesses of MBP,

MBP-1, MBP-2, and MBP-3 were 74, 59, 62, and 63μm, respectively.
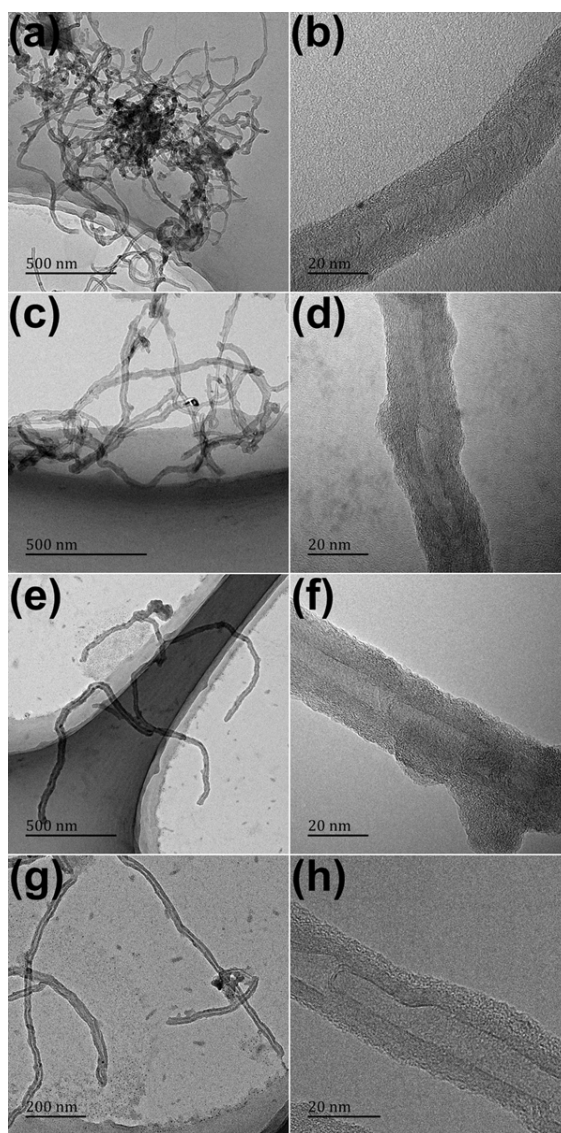
Figure 3. TEM images of (a, c) MWNTs, (c, d) PBI dispersed MWNTs with centrifugation

force of 954 g, (e, f) PBI dispersed MWNTs with centrifugation force of 3819 g, and (g, h,)

PBI dispersed MWNTs with centrifugation force of 8594 g.

14

3.2. Fabrication and characterization of buckypapers

Buckypapers were prepared by traditional paper-making process. From the photographs of buckypapers (Figure 4), it can be seen that MBP was brittle that fragmented upon drying because of the remained agglomerates and the relatively weak intertube interactions. While all the MWNTs/PBI papers were flexible without disruption. SEM images with low magnification (Figure 4a-4d) showed the surfaces of papers were relatively smooth because of the suction forces generated by the vacuum filtration. Moreover, the surfaces become more compact in MWNTs/PBI papers because of the presence of polymers. High magnification images (Figure 4e-4h) clearly demonstrated the differences among these papers. The junctions between individual tubes seemed more seamless with increased centrifugation force, the diameters of individual tubes also become larger from MBP to MBP-3. All of the phenomena were attributed to the thicker polymer coatings around the tubes, which were consistent with the TEM observations of MWNTs/PBI with different centrifugation force. To confirm this point, we carried out elemental analysis on the buckypapers, the results were listed in Table 1, from which we could calculate the amount of PBI in each paper. The weight ratios of elemental N in samples were used to estimate the weight percents of PBI in buckypapers. The nitrogen in pure PBI was founded to be 18.68 wt%, which was slightly lower than theoretical value of 19.72 wt%, the presence of oxygen in PBI was probably due to some impurities. As a result, the calculated amounts of PBI in MBP-1, MBP-2, and MBP-3 were 9.53 wt%, 13.33 wt%, and 15.74 wt%, respectively,

15

which were in agreement with our assumption, that is, with increased centrifugation force, MWNTs with more coated polymers were retained in dispersions. Such findings might be helpful to prepare MWNT papers with tailored properties. Moreover, from high magnification SEM images, we also noted that more ends of MWNTs could be found in MBP-2 (Figure 4g) as compared to MBP-1 (Figure 4f), and the ends of MWNTs were even more in MBP-3 (Figure 4h), indicating more short tubes were existed in samples prepared from dispersions obtained by higher centrifugation force. We have also carried out SEM characterization on the bottom side of the buckypapers, it was found that the images of bottom side of buckypapers were almost the same as those of the top side (images not shown). Figure 4i-4l showed the cross-sections of buckypapers. However, the cross-sections of buckypapers seemed not as uniform as the surfaces, which might be due to the brittle fracture of the cross-sections in contrast to suction-flattened paper surfaces. In addition, the tubes in MBP-1, MBP-2, and MBP-3 stacked more tightly than those in MBP, and the diameters of tubes in MBP-1, MBP-2, and MBP-3 appeared slightly larger than those in MBP, which were consistent with the observations from paper surfaces (Figure 4e-4h).
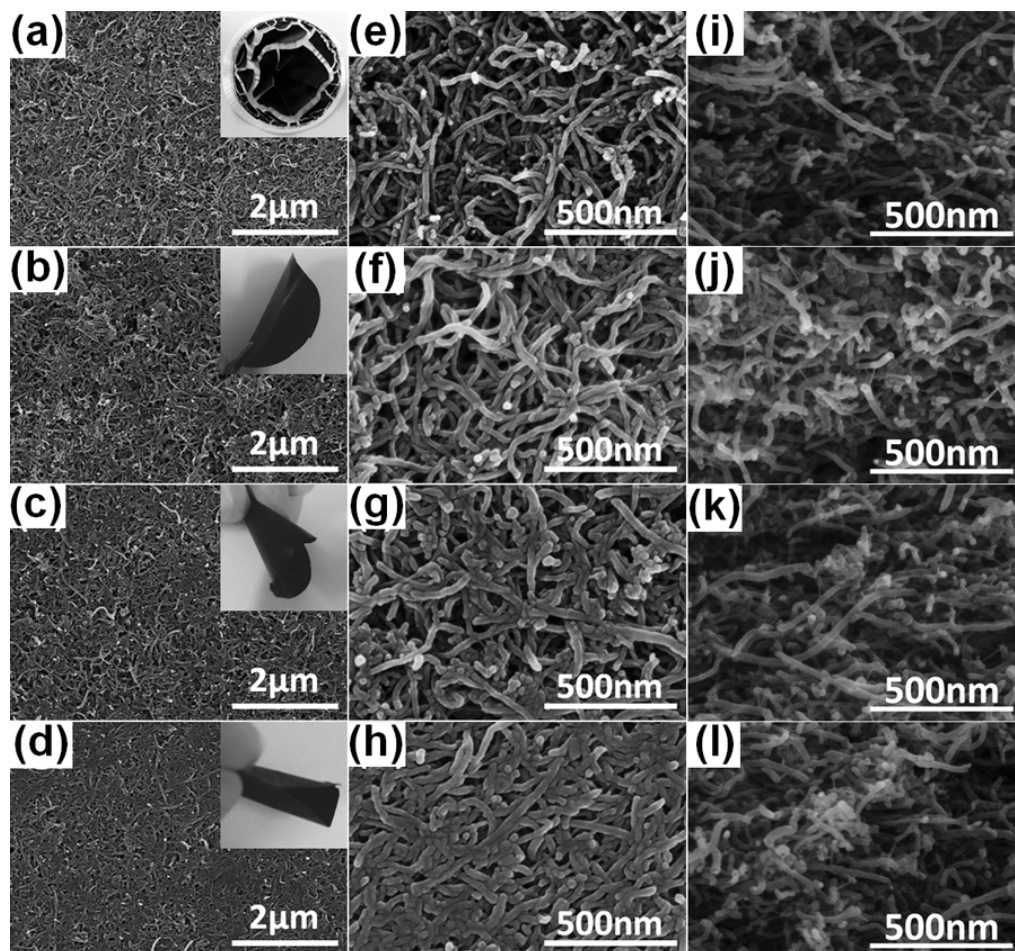
Figure 4. SEM images of the surface (a, e) and cross-section (i) of MBP, the surface (b, f) and cross-section (j) of MBP-1, the surface (c, g) and cross-section (k) of MBP-2, and the surface (d, h) and cross-section (l) of MBP-3. The insets showed the photographs of corresponding buckypapers.

Table 1. Elemental analysis data of buckypapers and PBI.

Sample	C(wt%)	H(wt%)	N(wt%)	O(wt%)
MBP	97.72	0.58	-	1.7
MBP-1	95.28	0.98	1.78	1.66
MBP-2	94.77	1.09	2.49	1.65
MBP-3	94.02	0.89	2.94	2.15
PBI	74.64	4.85	18.68	1.83

Raman spectra were then employed to characterize the buckypapers, as shown in Figure

5, from which we can see that the PBI showed no peak in the spectrum, while the disorder

mode (D-band) and the tangential mode (G-band) of MWNTs could be found in all

buckypapers, and the intensity ratios of D-band to G-band (I_D/I_G), which were usually used

as an indication for structural integration of graphitic carbons, were 1.559, 1.418, 1.448,

and 1.495 for MBP, MBP-1, MBP-2 and MBP-3, respectively. The decrease of I_D/I_G from

MBP to MBP-1 was attributed to the removal of amorphous carbons or impurities in raw

MWNTs, and the increase of I_D/I_G from MBP-1 to MBP-3 was due to the settlement of

longer MWNTs because of higher centrifugation force, thus left more open ends of

MWNTs in the papers. Nevertheless, this comparison showed our non-covalent process

preserved the integration of graphitic walls of MWNTs to a large extent. Moreover, we

found the position of G-band gradually shift from 1577 cm^{-1} in MBP to 1592 cm^{-1} in

MBP-3, which we attributed to the charge transfer from the CNTs to the conjugated

polymers, demonstrating again the interactions between MWNT and PBI[51, 52].
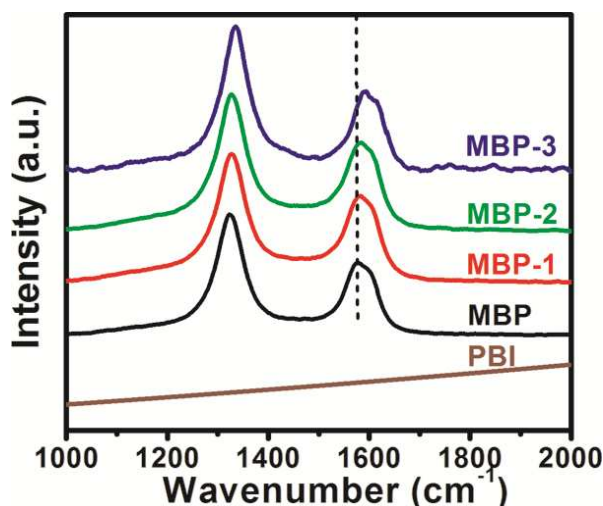
Figure 5. Raman spectra of PBI and buckypapers.

A major advantage for using high-performance aromatic polymer to prepare buckypaper is the preservation of the high thermal stability of CNTs. Therefore, we have investigate the thermal stabilities of buckypapers in air condition. Figure 6 presents the TGA and derivative thermogravimetry (DTG) curves of PBI and buckypapers. It was found that there was about 6.8% weight loss below 200 °C in PBI, which was ascribed to the elimination of bounded water in PBI. The maximum weight loss temperature (T_{max}) of PBI appeared at about 586.4 °C, which was in consistent with previously reported values for PBI in air[50], demonstrating its high thermal stability. The raw MBP also showed good thermal stability with almost no weight loss below 500°C. From DTG curve, the T_{max} can be found to be 600.5°C. To our surprise, the incorporation of PBI even improved the thermal stability of MBP. The T_{max} for MBP-1, MBP-2, and MBP-3 were 611.6, 621.7, and 612.5 °C,

19

respectively. We thought several reasons can be accounted for this observation: 1) the removal of less stable amorphous carbons or impurities by the non-covalent and centrifugation process; 2) as we have washed away the loosely attached polymers during the paper-making process, the strong interactions between MWNT and tightly adhered PBI could lower the decomposition rate of both MWNTs and polymers. In fact, maintaining or improving the thermal stability of buckypapers by polymer has rarely been reported in literatures, which was very important for the usage of buckypapers in high-temperature applications.
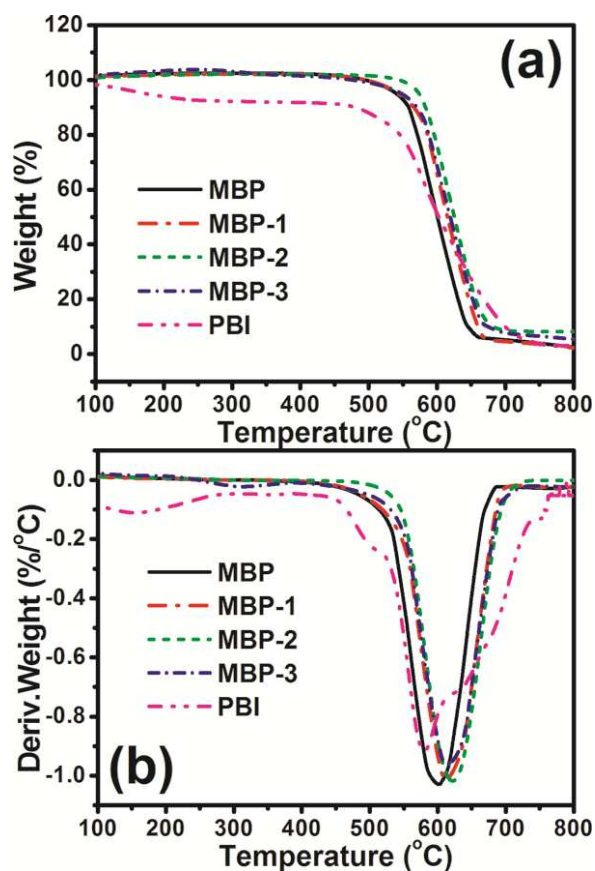
Figure 6. TGA (a) and DTG (b) curves of PBI and buckpapers.

Then the mechanical and electrical properties of buckypapers were evaluated, the resulted values of modulus, strength, ultimate strain, and electrical conductivity of each papers were compared in Figure 7 and listed in Table 2. It should be noted that as the MBP was too brittle to be handled in tensile test, so the mechanical properties of MBP were not included. From the comparison, it can be seen that MBP-2 shows the best mechanical properties with modulus, strength, and ultimate strain of 0.81 GPa, 8.1 MPa, and 3.2 %, respectively, which were higher than some buckypapers made from oxidized MWNTs[53] or small molecule cross-linked MWNTs[54, 55], demonstrating the effective reinforcement of PBI to MWNT papers. Moreover, it was found that the fabrication process has also influenced the final properties of buckypapers. For example, due to the removal of less functionalized MWNTs in MBP-2, the mechanical properties of MBP-2 were higher than MBP-1. While too high centrifugation force would remove longer MWNTs as in the case of MBP-3, so the mechanical properties of MBP-3 were also lower than MBP-2.

However, in contrast to the improved thermal and mechanical properties, the electrical conductivities of buckypapers were deteriorated by the introduce of polymers. The conductivity decreased from 30.0 S/cm of MBP to 8.14 S/cm of MBP-1, and then dramatically decreased to 0.21 and 0.18 S/cm in MBP-2 and MBP-3. It is noted that in the study of Chan-Park et al.[51], the conductivity of MWNTs/Polyimide composites could reach 38.8 S/cm with 30 wt% MWNTs. However, the conductivities of our composite

papers were much lower even with more than 85wt% MWNTs. Besides the intrinsic

lower conductivity of our MWNTs, the major reason was thought to be the efficient

wrapping of MWNTs by PBI, which hindered the electron transport among MWNTs.
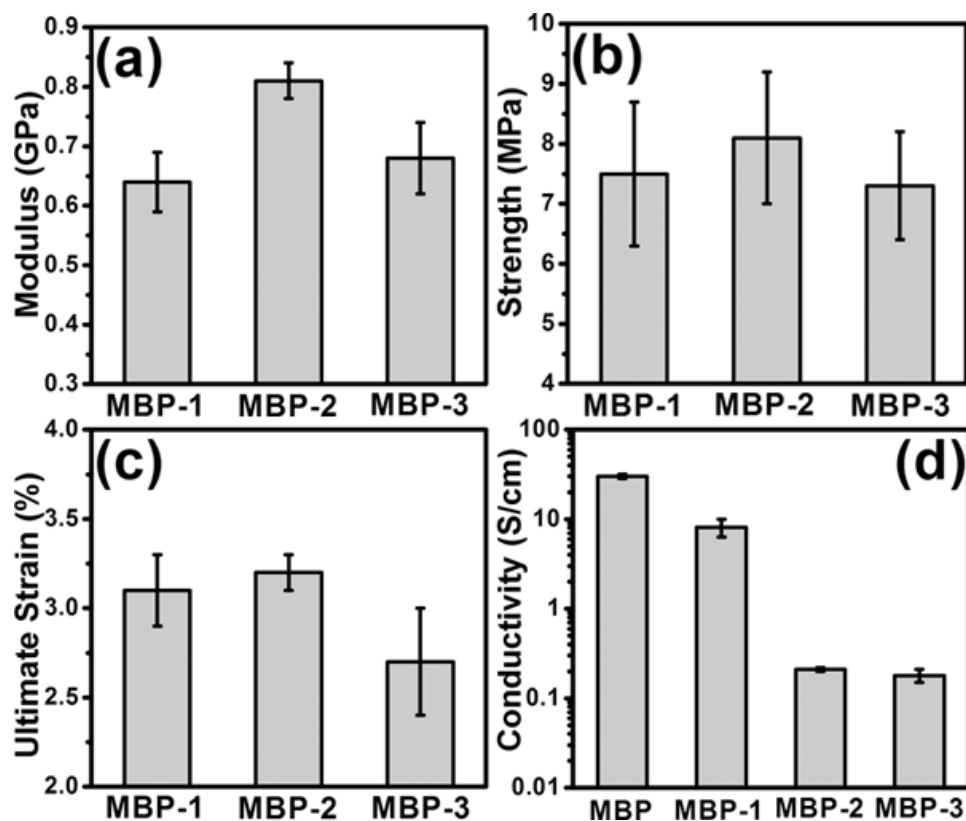
Figure 7. Comparisons of the (a) modulus, (b) strength, (c) ultimate strain, and (d)

electrical conductivity of buckypapers.

Table 2. Tensile properties, thermal stabilities and conductivity of buckypapers.

Sample	Young's Modulus (GPa)	Tensile Strength (MPa)	Ultimate Strain (%)	T_{max} (°C)	Conductivity (S/cm)
MBP	-	-	-	600.5	30.0±1.5
MBP-1	0.64±0.05	7.5±1.2	3.1±0.2	611.6	8.14±1.81
MBP-2	0.81±0.03	8.1±1.1	3.2±0.1	621.7	0.21±0.01
MBP-3	0.68±0.06	7.3±0.9	2.7±0.3	612.5	0.18±0.03

3.3 Fabrication and characterization of Ag/buckypaper hybrids.

As the imidazole group could coordinate metal centre through its amino heteroatom[44-46], it is thought that MNPs could be easily deposited onto our PBI reinforced buckypapers. So we next investigated the formation and properties Ag/buckypaper hybrids. MBP-2 was used as model substrate because of its better mechanical properties, PBI and MBP were also used as a reference. All hybrids were prepared by adsorption-reduction process. Figure 8 shows the corresponding Ag/PBI, Ag/MBP and Ag/MBP-2. When immersed the substrates in AgNO$_3$ solution for 2h and then reduced, AgNPs were uniformly deposited on the surface of PBI (Figure 8a and 8b), the sizes of most AgNPs were 20~50 nm with some occasionally appeared larger particles (less than 100 nm), demonstrating the coordination ability of PBI to silver ions and AgNPs. However, irregular large particles with sizes of

several hundreds nanometers were attached on the surface of MBP (Figure 8c and 8d), which might be due to the lack of interaction between MWNTs and AgNPs. In contrast, AgNPs with much smaller sizes were evenly deposited on MBP-2 (Figure 8e and 8f), demonstrating the positive effect of PBI on the formation of uniform Ag/buckypaper hybrids. Energy Dispersive Spectroscopy (EDS) showed that about 1.14 wt% Ag were presented in this sample. Increasing the immersion time of MBP-2 in $AgNO_3$ solution to 24h further increased the deposited AgNPs, as demonstrated in Figure 8g and 8h, EDS suggested about 4.43 wt% AnNPs were deposited, demonstrating the controlled deposition of Ag on MBP-2. Due to the higher loading of AgNPs on Ag/MBP-2 with immersion time of 24h, we would carry out further characterizations on this sample.

Figure 9a shows an enlarged SEM image of Ag/MBP-2, from which we can calculate the size distribution of AgNPs. The statistics of sizes from a large number (~180 pieces) of particles are presented in Figure 9b. Based on the size statistical analysis, it is found that the diameter of most AgNPs (~87.3%) are smaller than 50nm, and about 72.8% of AgNPs were in the region of 35~50 nm, suggesting the uniform size distribution. The average size were found to be even smaller than AgNPs deposited on polydopamine-coated graphene paper (~80 nm)[51], demonstrating again the strong interaction between Ag ions and PBI. Figure 9c shows the XRD pattern of Ag/MBP-2, the peak at 2θ=25.9° were attributed to the (002) planes of MWNTs. The smaller peaks at 2θ=38.0°, 44.0°, 64.6°, and 77.3° were assigned to the (111), (200), (220), and (311) planes of face-centered cubic (fcc) silver, which were

identical to previously reported values for crystalline AgNPs[56, 57].
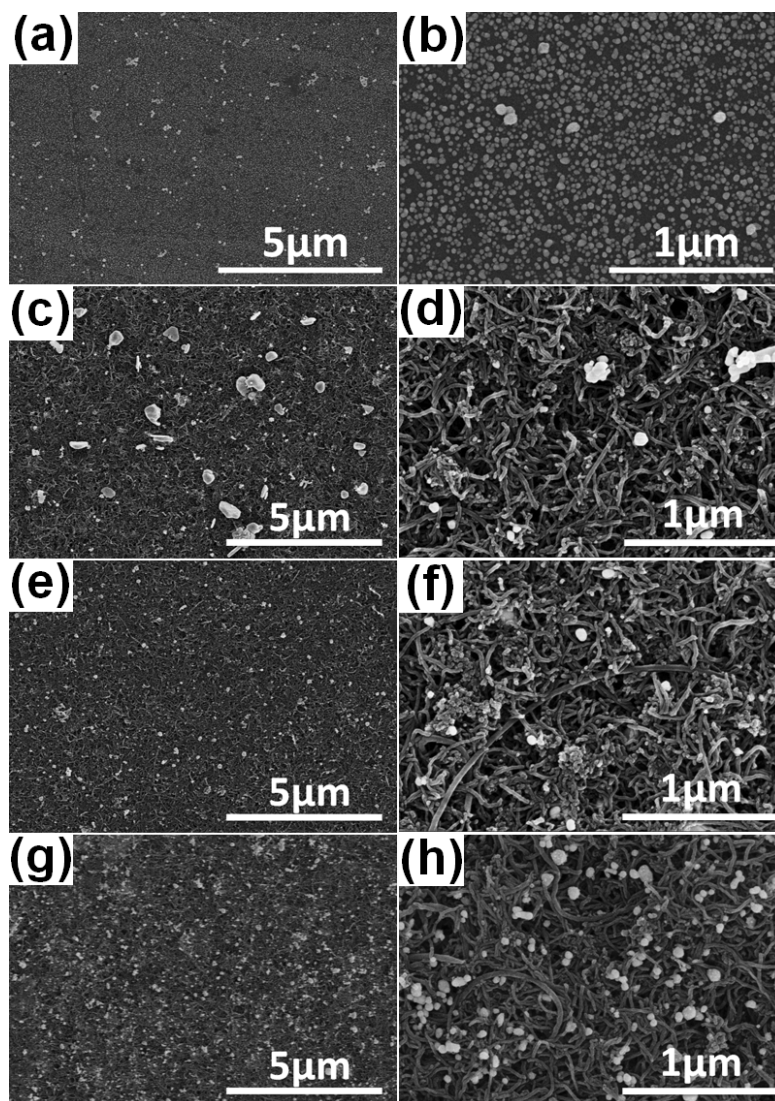
Figure 8. SEM Images of (a, b) Ag/PBI with immersion time of 2h, (c, d) Ag/MBP with immersion time of 2h, (e, f) Ag/MBP-2 with immersion time of 2h, and (g, h) Ag/MBP-2 with immersion time of 24h.
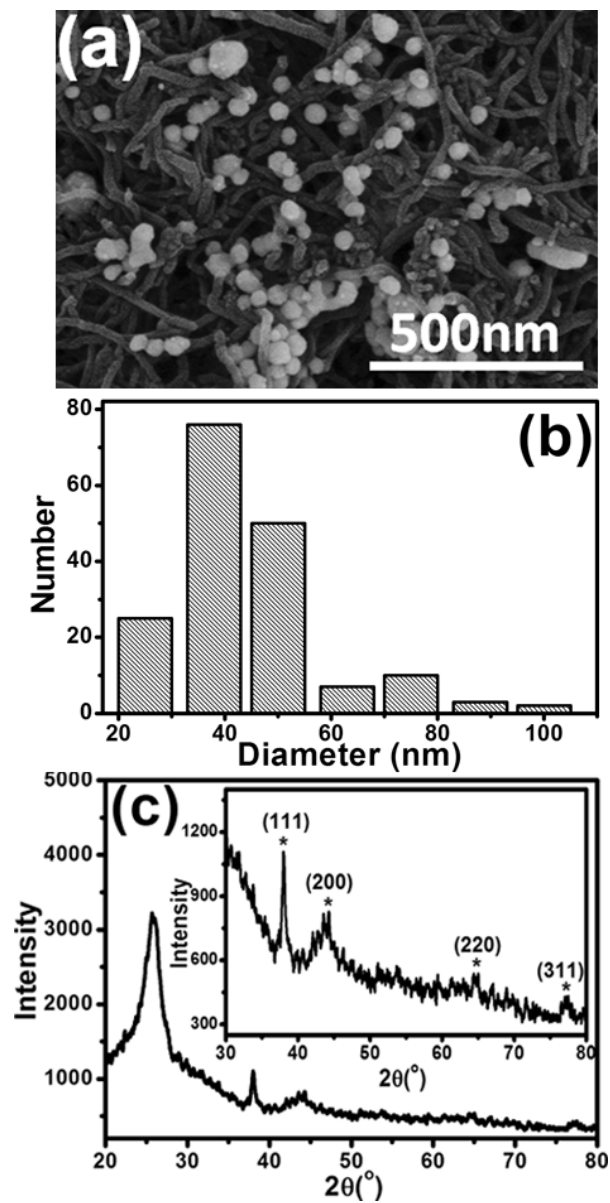
Figure 9. SEM image of Ag/MBP-2 with high magnification. (b) Size distribution of

AgNPs in Ag/MBP-2 based on SEM images. (c) XRD pattern of Ag/MBP-2.

The mechanical and electrical properties of Ag/MBP-2 were also evaluated. The modulus,

strength, and ultimate strain of Ag/MBP-2 were found to be 0.51GPa, 6.41MPa, and 2.43%,

respectively, which were slightly lower than those of MBP-2. However, the electrical

conductivity of MBP-2 were dramatically increased from 0.21 to 24.2 S/cm after deposition

of AgNPs, suggesting the reconstruction of conductive network in Ag/MBP-2.

3.4. Catalysis applications of Ag/buckypaper hybrids.

AgNPs have been frequently used as catalyst since their high reactivity and selectivity.

However, due to the problem of aggregation in small AgNPs during catalysis, and the

difficulty in recovery of catalyst, AgNPs were usually immobilized on suitable solid

substrate to maintain their high activity and facilitate their recycling. Due to the stability of

both MWNTs and PBI in harsh chemical environment, it was expected that our Ag/MBP-2

could serve as reusable catalyst. Here we have chosen the reduction of 4-nitrophenol (4-NP)

to 4-aminophenol (4-AP) as a model reaction. The initial concentration of $NaBH_4$ was set to

be much higher than 4-NP to make the reaction follow pseudo-first-order kinetics[58, 59]. The

reduction process was monitored by UV-vis spectra, as shown in Figure 10a. It can be seen

that the intensity of characterized peak at 400nm for 4-nitrophenolate ions gradually

disappeared as the reduction processed. Meanwhile, a new peak at 295nm, which was

attributed to 4-AP, was progressively established, demonstrating the reduction of 4-NP and

formation of 4-AP. After 55 min reaction, the solution become colorless, indicating the

complete conversion of 4-NP. Since the concentration of 4-NP in solution at given time is

proportional to the absorbance, the rate constant (k) can be determined from the linear plot

of $\ln(A_t/A_0)$ against the reaction time, where A_t is the absorbance of solution at time (t), and

A_0 is the absorbance of the solution at reaction t=0, Figure 1b showed the k thus obtained is 0.0588 min^{-1}. Considering the Ag/MBP-2 used in the reduction process was 1 mg, and the content of Ag in Ag/MBP-2 was 4.43wt%, the true activity parameter (κ) of AgNPs on Ag/MBP-2, which represents the ratio of k to the mass of catalyst, was about 22.21 S^{-1} g^{-1}. The relatively high κ of our AgNPs supported on MBP-2 as compared to some polymer-coated AgNPs[60] or AgNPs supported on spherical substrate[61, 62] suggested that the PBI attached on MWNTs can effectively prevent AgNPs from aggregation and maintain their high catalytic activity.

To investigate the reusability of the catalyst, we have carried out five successive catalysis process on the same catalyst. After one cycle of catalysis, the Ag/MBP-2 was taken out of the solution, washed with water and dried, and then for the next cycle of catalysis. The absorbance for each cycle was measured at the same time as the first cycle. The test results show that the catalyst still exhibit relatively high activity as the conversion was only slightly lowered to 86.3% after five times catalysis. SEM image of Ag/MBP-2 after five cycles of catalysis (Figure 10d) showed that some large clusters with sizes up to micrometers were formed, which might be accounted for the lowered catalytic activity. However, it should be noted that the Ag/MBP-2 maintained its integration during the whole test process, as no cracks could be found from the image. Such results show that MBP-2 could act as reliable and easily reusable substrate for supporting AgNPs for catalysis application.
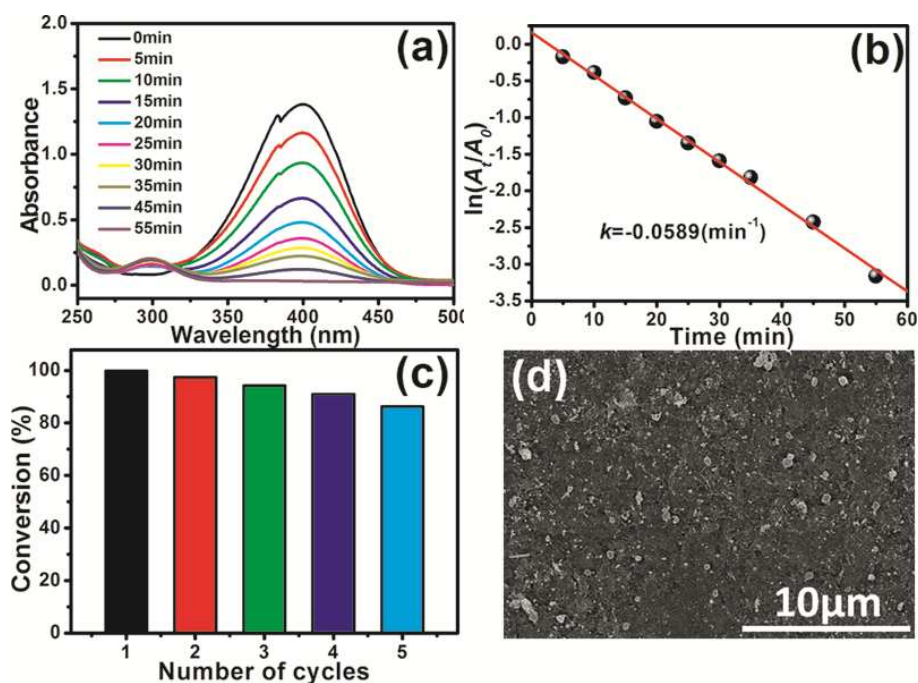
Figure 10. (a) UV-vis spectra of 4-nitrophenol reduced by sodium borohydride in the presence of Ag/MBP-2. (b) Plot of $\ln(A_t/A_0)$ against the reaction time. (c) The conversion of 4-nitrophenol as a function of cycles. (d) SEM image of Ag/MBP-2 after five cycles of catalysis.

4.Conclusions

We reported the fabrication of MWNT buckypapers and their hybrids with AgNPs with the assist of PBI. PBI was a high-performance aromatic polymer that could effectively and homogeneously disperse MWNTs in organic solvent with concentrations as high as 1.6 mg/mL, which greatly facilitated the process of MWNT-based macroscopic materials. With the help of PBI, free-standing and flexible papers with good mechanical properties can be

29

prepared by facile filtration method in contrast to fragile paper prepared from pure MWNTs. The thermal stability of MWNT paper was also improved by the introduction of PBI due to the inherent excellent thermal stability of PBI and the strong interactions between MWNTs and PBI, which was very important for use of buckypapers in high-temperature applications. In contrast, the electrical conductivities of MWNTs/PBI papers were lower than MWNT paper due to the wrapping of PBI on MWNTs. Moreover, the centrifugation force applied to obtain homogeneous dispersion of MWNTs was found to be an important parameter for the final performance of thus-obtained papers, as the centrifugation force could influence the attached amount of polymers and the geometrical morphologies of the dispersed MWNTs. Because of the coordination effect of PBI to the metal ions, AgNPs with relatively uniform sizes in the region of 35~50nm were then homogenously deposited on MWNTs/PBI papers. The deposited AgNPs increased the conductivity of MWNTs/PBI paper by several orders of magnification. Catalysis experiments also demonstrated the good catalytic activity and recyclability of our Ag/buckypaper hybrids. All results demonstrated the great potential of PBI as an effective dispersant for fabrication of high-performance MWNT buckypapers and multifunctional Ag/buckypapers hybrids.

Acknowledgment

References

1. Z. Spitalsky, T. Dimitrios, P. Konstantinos and G. Costas, *Prog. Polym. Sci.*, 2010, **35**, 357–401;

2. J. N. Coleman, U. Khan and Y. K. Gun'ko, *Adv. Mater.*, 2006, **18**, 689–706;

3. M. Moniruzzaman and K. I. Winey, *Macromolecules*, 2006, **39**, 5194–5205;

4. L.Q. Liu, W. J. Ma and Z. Zhang, *Small*, 2011, **7**, 1504–1520;

5. H. D. Espinosa, T. Filleter and M. Naraghi, *Adv. Mater.*, 2012, **24**, 2805–2823;

6. H. Qian, E. S. Greenhalgh, M. S. P. Shaffer and A. Bismarck, *J. Mater. Chem.*, 2010, **20**, 4751–4762;

7. J. W. Zhang, D. Z. Jiang and H. X. Peng, *RSC Adv.*, 2013, **3**, 15290–15297;

8. S. Roy, V. Jain, R. Bajpai, P. Ghosh, A. S. Pente, B. P. Singh and D. S. Misra, *J. Phys. Chem. C*, 2012, **116**, 19025–19031;

9. K. Evanoff, J. Benson, M. Schauer, I. Kovalenko, D. Lashmore, W. J. Ready and G. Yushin, *ACS Nano*, 2012, **6**, 9837–9845;

10. J. W. Zhang, D. Z. Jiang, H. X. Peng and F. X. Qin, *Carbon*, 2013, **63**, 125–132;

11. J. Liu, A. G. Rinzler, H. Dai, J. H. Hafner, R. K. Bradley, P. J. Boul, A. Lu, T. Iverson, K. Shelimov, C. B. Huffman, F. R. -Macias, Y.-S. Shon, T. R. Lee, Da. T. Colbert and R. E.

Smalley, *Science*. 1999, **280**, 1253–1256;

12. S. M. Cooper, H. F. Chuang, M. Cinke, B. A. Cruden, and M. Meyyappan, *Nano Lett.*, 2003, **3**, 189–192;

13. I. W. P. Chen, *Chem. Commun.*, 2013, **49**, 2753–2755;

14. G. H. Chen, D. N. Futaba, S. Sakurai, M. Yumura and K. Hata, *Carbon*, 2014, **67**, 318–325;

15. I. W. P. Chen, R. Liang, H. Zhao, B. Wang and C. Zhang, *Naotechnology*, 2011, **22**, 485708;

16. Q. Cao and J. A. Rogers, *Adv. Mater.*, 2009, **21**, 29–53;

17. L. Liu, W. Ma, and Z. Zhang, *Small* 2011, **7**, 1504–1520;

18. D. Tuncel, *Nanoscale*, 2011, **3**, 3545–3554;

19. Z. X. Song, J. J. Dai, S. Zhao, Y. Zhou, F. Su, J. Cui and Y. H. Yan, *RSC Adv.*, 2014, **4**, 2327–2338;

20. N. R. Tummala, B. H. Morrow, D. E. Resasco and A. Striolo, *ACS Nano*, 2010, **4**, 7193–-7204;

21. L. Vaisman, H. D. Wagner and G. Marom, *Adv. Colloid Interface Sci.*, 2006, **128–130**, 37–46;

22. Q. L. Liu, M. Li, Z. Z. Wang, Y. Z. Gu, Y. X Li and Z. G. Zhang, *Composites Part A*, 2013, **55**, 102–109;

23. A. Satti, A. Perret, J. E. McCarthy and Y. K. Gun'ko, *J. Mater. Chem.*, 2010, **20**,

7941–7943;

24. J. Boge, L. J. Sweetman, M. Panhuis and S. F. Ralph, *J. Mater. Chem.*, 2009, **19**, 9131–9140;

25. A. Aldalbahi, M. Panhuis, *Carbon*, 2012, **50**, 1197–1208;

26. J. Li, Y. Gao, W. Ma, L. Liu, Z. Zhang, Z. Niu, Y. Ren, X. Zhang, Q. Zeng, H. Dong, D. Zhao, L. Cai, W. Zhoua and S. Xie, *Nanoscale*, 2011, **3**, 3731–3736;

27. Z. Wang, Z. Liang, B. Wang, C. Zhang and L. Kramer, *Compos. Part A*, 2004, **35**, 1225–1232;

28. S. Wang, Z. Liang,G. Pham, Y. -B. Park, B. Wang, C. Zhang, L. Kramer and P. Funchess, *Nanotechnology*, 2007, **18**, 095708;

29. G. T. Pham, Y. -B. Park, S. Wang, Z. Liang, B. Wang, C. Zhang, P. Funchess and L. Kramer, *Nanotechnology*, 2008, **19**, 325705;

30. A. M. Díez-Pascual, J. Guan, B. Simard, M. A. Gómez-Fatou, *Compos. Part A*, 2012, **43**, 997–1006;

31. A. M. Díez-Pascual, J. Guan, B. Simard, M. A. Gómez-Fatou, *Compos. Part A*, 2012, **43**, 1007–1015;

32. M. T. Byrne, C. A. Hanley and Y. K. Gun'ko, *J. Mater. Chem.*, 2010, **20**, 2949–2951;

33. C. F. McAndrew and M. Baxendale, *Nanotechnology*, 2013, **24**, 305202;

34. D. N. Ventura, S. Li, C. A. Baker, C. J. Breshike, A. L. Spann, G. F. Strouse, H. W. Kroto and S. F. A. Acquah, *Carbon*, 2012, **50**, 2672–2674;

35. H. T. Wang, Z. X. Dong and C. Z. Na, *ACS Sustainable Chem. Eng.*, 2013, **1**, 746–752;

36. M. P. Sk, C. K. Jana and A. Chattopadhyay, *Chem. Commun.*, 2013, **49**, 8235–8237;

37. Y. P. Huang, H. Ma, S. G. Wang, M. W. Shen, R. Guo, X. Y. Cao, M. F. Zhu and X. Y. Shi, *ACS Appl. Mater. Interfaces*, 2012, **4**, 3054–3061;

38. Z. M. Wang, C. L. Xu, G. Q. Gao and X. Li, *RSC Adv.*, 2014, **4**, 13644–13651;

39. Y. Wang, Z. X. Shi, J. H. Fang, H. J. Xu and J. Yin, *Carbon*, 2011, **49**, 1199–1207;

40. Y. Wang, J. R. Yu, L. Chen, Z. M. Hu, Z. X. Shi and J. Zhu, *RSC Adv.*, 2013, **3**, 20353–20362;

41. K. Matsumoto, T. Fujigaya, K. Sasaki and N. Nakashima, *J. Mater. Chem.*, 2011, **21**, 1187–1190;

42. M. Okamoto, T. Fujigaya and N. Nakashima, *Small*, 2009, **5**, 735–740;

43. T. Fujigaya and N. Nakashima, *Adv. Mater.*, 2013, **25**, 1666–1681;

44. A. A. D'Archivio, L. Galantini, A. Biffis, K. Jeřábek and B. Corain, *Chem. Eur. J.*, 2000, **6**, 794–799;

45. B. K. Balan, V. S. Kale, P. P. Aher, M. V. Shelke, V. K. Pillai and S. Kurungot, *Chem. Commun.*, 2010, **46**, 5590–5592;

46. B. K. Balan, H. D. Chaudhari, U. K. Kharul and S. Kurungot, *RSC Adv.*, 2013, **3**, 2428–2436;

47. M. Lv, S. Su, Y. He, Q. Huang, W. B. Hu, D. Li, C. H. Fan and S. T. Lee, *Adv. Mater.*, 2010, **22**, 5463–5467;

48. S. Wunder, F. Polzer, Y. Lu, Y. Mei and M. Ballauff, *J. Phys. Chem. C*, 2010, **114**, 8814–8820;

49. M. M. Zhu, C. J. Wang, D. H. Meng and G. W. Diao, *J. Mater. Chem. A*, 2013, **1**, 2118–2125;

50. M. Okamoto, T. Fujigaya and N. Nakashima, *Adv. Funct. Mater.*, 2008, **18**, 1776–1782;

51. W. Yuan, J. F. Che and M. B. C. Park, *Chem. Mater.*, 2011, **23**, 4149–4157;

52. W. Yuan, W. F. Li, Y. G. Mu and M. B. C. Park, *ACS Appl. Mater. Interfaces*, 2011, **3**, 1702–1712;

53. Z. Špitalský, C. Aggelopoulos, G. Tsoukleri, C. Tsakiroglou, J. Parthenios, S. Georga, C. Krontiras, D. Tasis, K. Papagelis and C. Galiotis, *Mater. Sci. Eng., B*, 2009, **165**, 135–138;

54. S. Steiner, S. Busato and P. Ermanni, *Carbon*, 2012, **50**, 1713–1719;

55. D. N. Ventura, R. A. Stone, K. S. Chen, H. H. Hariri, K. A. Riddle, T. J. Fellers, C. F. Strouse, H. W. Kroto and S. F. A. Acquah, *Carbon*, 2010, **48**, 987–994;

56. S. K. Li, Y. X. Yan, J. L. Wang and S. H. Yu, *Nanoscale*, 2013, **5**, 12616-12623;

57. H. Zhao, H. Fu, T. Zhao, L. Wang and T. Tan, *J. Colloid Interface Sci.*, 2012, **375**, 30–34;

58. H. S. Shin and S. Huh, *ACS Appl. Mater. Interfaces*, 2012, **4**, 6324–6331;

59. B. Liu, J. C. Wang, S. X. Sun, X. M. Wang, M. Zhao, W. Zhang, H. Zhang and X. L. Yang, *RSC Adv.*, 2013, **3**, 18506–18518;

60. M. H. Rashid and T. K. Mandal, *J. Phys. Chem. C*, 2007, **111**, 16750–16760;

61. Y. Chi, Q. Yuan, Y. J. Li, J. C. Tu, L. Zhao, N. Li and X. T. Li, *J. Colloid Interface Sci.*, 2012, **383**, 96–102;

62. S. C. Tang, S. Vongehr and X. K. Meng, *J. Phys. Chem. C*, 2010, **114**, 977–982.